Journal of Materials Research, Vol. 15, 546-553, 2000.

The influence of oxide and adsorbates on the nanomechanical response of silicon surfaces

S.A. Syed Asif*, K.J. Wahl and R.J. Colton
Code 6170, Chemistry Division, Naval Research Laboratory, Washington, DC 20375-5342
**Materials Science and Engineering, University of Florida, Gainesville, FL 32611*

In this article we report the influence of surface oxides and relative humidity on the nanomechanical response of hydrophobic and hydrophilic Si surfaces. Depth-sensing nanoindentation combined with force modulation enabled measurement of surface forces, surface energy, and interaction stiffness prior to contact. Several regimes of contact were investigated: pre-contact, apparent contact, elastic contact, and elasto-plastic contact. Both humidity and surface preparation influenced the surface mechanical properties in the pre- and apparent-contact regimes. Meniscus formation was observed for both hydrophobic and hydrophilic surfaces at high humidity. Influence of humidity was much less pronounced on hydrophobic surfaces and was fully reversible. In the elastic and elasto-plastic regimes, the mechanical response was dependent on oxide layer thickness. Irreversibility at small loads (300 nN) was due to the deformation of the surface oxide. Above 1 μN, the deformation was elastic until the mean contact pressure reached 11 GPa, whereby Si underwent a pressure-induced phase transformation resulting in oxide layer pop-in and breakthrough. The critical load required for pop-in was dependent on oxide thickness and tip radius. For thicker oxide layers, substrate influence was reduced and plastic deformation occured within the oxide film itself without pop-in. Elastic modulus and hardness of both the oxide layer and Si substrate were measured quantitatively for depths <5 nm.

KEYWORDS: nanoindentation, humidity, silicon, SiO_2

I. INTRODUCTION

Recently there has been an increased interest in studying the mechanical properties of extremely small volumes of materials, e.g., thin films, surface coatings, and nanostructures over the length scale of a few nanometers. For sub-micron scale mechanical property measurements, depth sensing nanoindentation techniques are very successful and gaining much attention[1]. However, for ultra-small volumes of materials below a length scale of 10 nm, measuring the quantitative mechanical properties of materials is extremely difficult even using depth-sensing nanoindentation. There are many reasons: difficulty in characterizing the tip shape, unknown thermal drift, floor noise, and poor surface sensitivity of the indentation instrument. To detect the specimen surface, most of the nanoindentation instruments require a minimum of 1 micro Newton (μN) contact load before applying the test load. Hence, for compliant materials the indenter will penetrate the specimen tens of nanometers and unknown contact damage may occur.

To measure the response of monolayers or nanometer thick surface layers, the measuring instrument must have good surface sensitivity. The atomic force microscope (AFM)[2] has very good surface sensitivity and has been shown[3-5] to measure nanomechanical properties. However cantilever instability, conventional force detection techniques (inferred from the known spring constant of the lever), small tip size, and unknown tip shape, make contact area measurements difficult, hence the measured mechanical properties are usually only qualitative. To avoid this problem, we have recently implemented a force modulation technique coupled with nanoindentation using a three-plate capacitive load-displacement transducer[6]. The stiffness sensitivity of the instrument is ~0.1 N/m, sufficient to detect long-range surface forces and locate the surface of the specimen.

Silicon is one of the most widely used and studied materials for numerous applications and devices. It is also used as a moving micromechanical element in micro-electromechanical (MEMS) devices[7]. Thus it is important to understand the effect of surface treatments, surface chemistry, and environmental conditions on the nanomechanical response of Si surfaces. In this article we report the influence of surface oxides and relative humidity on the nanomechanical response of Si surfaces using a combined depth sensing and force modulation technique. With this technique we have measured the mechanical response of silicon surfaces in four different regimes: pre-contact, apparent contact, elastic contact and elasto-plastic contact. In the elastic and elasto-plastic contact regimes, we have measured the mechanical properties of the surface oxide layer quantitatively for contact depths less than 5 nm. We show that the oxide layer on the Si surface is more compliant than the Si substrate and the mechanical response is dependent on thickness of the oxide layer.

II. EXPERIMENTAL

The material used for this study was a Si single crystal wafer with the (100) plane normal to the test surface. Two types of Si surfaces were prepared: hydrophilic and

hydrophobic. Hydrophilic surfaces were prepared using a piranha etch (70% H_2SO_4 +30% H_2O_2) for 30 minutes and then rinsed immediately in triply distilled water for five minutes and finally dried in nitrogen. This etching procedure leaves the surface with a 5 nm thick oxide layer measured using an ellipsometer. The water contact angle measured with a goniometer was 5^o.

Hydrophobic surfaces were obtained by etching the Si using 40% HF for 10 minutes, rinsing in 4:1 CH_3OH:H_2O for six minutes, rinsing in CH_3OH for another six minutes, and finally drying in nitrogen. This etching procedure removes the oxide layer (or reduces its thickness)[8]. The thickness of the oxide layer was < 1nm and the contact angle measured is 75^o which confirms the surface is hydrophobic. A Si wafer (100) with a 30 nm thermally grown oxide layer was also examined. Prepared specimens were placed immediately inside a glove box with <2% RH and the experiments done within a few minutes of surface preparation.

The experiments are carried out using a modified Hysitron picoindenter with a Berkovich diamond tip. Detailed descriptions of the instrument and calibration procedures are given elsewhere[6]. The indenter tip shape is calibrated with a fused quartz specimen using standard procedures[9]. The tip surface has not been modified with the exception of cleaning by swabbing with CH_3OH and drying in nitrogen.

Contact stiffness is measured using a force modulation technique, where a small sinusoidal AC force ranging between 20-150 nN (peak-to-peak) at 110-132 Hz is added to the applied force. The resulting oscillation in displacement and the phase shift between force and displacement are monitored using a lock-in amplifier. The displacement amplitude and phase shifts are used to calculate the contact stiffness. For pre-contact and apparent contact experiments the specimen approaches the indenter tip using the AFM Z piezo[6] at an approach rate of 0.5 nm/s until the phase shift reaches the preset value. Then the specimen is withdrawn at the same rate until the phase shift reaches the original value.

For indentation experiments, the same phase shift detection technique[6] during approach is used to detect the surface of the specimen before applying a load. The indentation experiments are carried out in a loading and unloading sequence in load- control mode using the load-displacement transducer. To study the effect of humidity and surface preparation all the experiments are carried out inside a dry N_2 –purged glove box with humidity control. The N_2 flowed through a column of $CaSO_4$ and 5 nm molecular sieve to eliminate H_2O and organic impurities. The specimen and the instrument reached thermal equilibrium with thermal drift <0.05 nm/s before indentation tests were performed.

III. RESULTS AND DISCUSSION

A. Dynamic response

Figure 1 shows the dynamic response of the indenter system when it is free of contact. The top part of the curve plots dynamic compliance (the ratio of the displacement amplitude to the force amplitude) as a function of frequency. The resonance can be clearly seen around 691 rad/s. The bottom part of the curve shows the phase shift as a function of frequency. The phase shift plotted here is the measured phase shift due to electronics (filters) and mechanical damping by the capacitance plate. The important point to note in Fig. 1 is the large phase shift at resonance. This implies that when the driving frequency is close to the resonance frequency in an experiment, any change in dynamic compliance due to tip surface interaction will result in a large phase shift. For example, if the driving frequency is slightly less than the resonance frequency (110 Hz) during tip-specimen approach, shown as a dotted line in Fig. 1, an increasing attractive force (positive force gradient) between the tip and specimen surface will shift the resonance frequency to lower frequency[10]. This will lead to an increase in dynamic compliance (or decrease in interaction stiffness) and decrease in phase (Fig. 1). As the surface comes closer, there will be repulsive interaction between the tip and surface, leading to an increase in interaction stiffness and increase in phase shift. Thus it is possible to observe the tip-surface interaction (or the pre-contact response) during approach to contact.

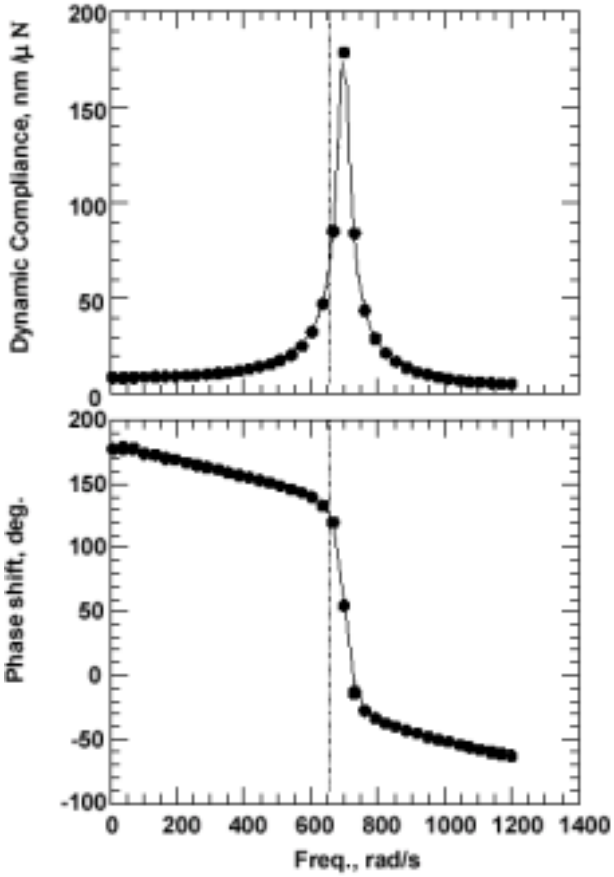

FIG.1. Dynamic response of the indenter system: a) dynamic compliance and b) phase shift.

B. Force and interaction stiffness curve: Pre- and apparent contact

Figure 2 shows the typical force and interaction stiffness curves during approach and retraction for an as-received Si

surface with the native oxide layer intact under ambient conditions (54% RH). The force curve shown here is similar to the force curve measurement in AFM[3]. The interaction stiffness is a convolution of force gradient and contact stiffness between the tip and surface. More work is in progress for the complete interpretation of these interaction stiffness curves. In general, the force curves can be divided into three regimes: pre-contact, apparent- or intermittent-contact, and elastic or elasto-plastic contact regimes as shown in Fig. 2. The attractive interaction is negative (A-C, A'-C') and the repulsive interaction is positive (C-D, C' and beyond). The tip experienced a maximum attractive force of 140 nN and interaction stiffness of -3 N/m. The maximum (B') attractive interaction stiffness (the force gradient at point B) is less than the spring stiffness of the indenter (132 N/m), hence there is no mechanical instability.

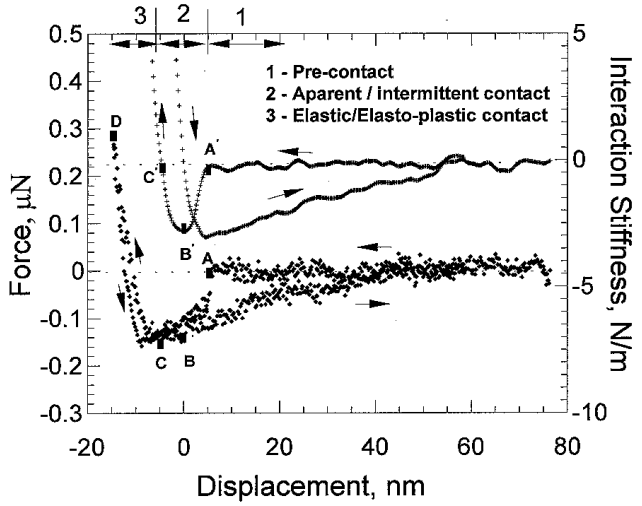

FIG. 2. Force (♦) and interaction stiffness (+) curves during approach (←) and retraction (→).

From the force curve measurement the surface energy of the sample can be calculated using the following equation[11]

$$F = 4\pi R\gamma \qquad (1)$$

where F is the attractive force, γ is the surface energy, and R (~200 nm) is the radius of curvature of the tip (assuming sphere on flat geometry). The calculated surface energy of 60-80 mJ/m^2 is in good agreement with the surface energy of water (72 mJ/m^2)[11]. This is expected as the experiments are conducted under ambient conditions with a relative humidity of 54%.

As the distance between the sample and tip is reduced, the repulsive interaction increases and the tip comes in contact with the sample resulting in indentation (C-D). The maximum load applied to the sample surface during contact is 300 nN. At point D in Fig. 2, the sample direction is reversed such that the sample moves away from the indenter. During retraction, hysteresis in the force and interaction stiffness curve can be seen in both contact (indentation) and attractive regimes. Although hysteresis can occur due to experimental artifacts such as piezo creep and improper lock-in time constants, care was taken to avoid these artifacts. In the contact regime, for a maximum load of 300 nN (point D) the unloading is not reversible and the deformation is not elastic. This type of behavior was found for loads less than 500 nN and varied for different samples and location. The variation could be due to the localized deformation of the contaminant surface layer, which is not uniformly covering the oxide surface. In the force curve measurement, the hysteresis during pull-off (attractive regime) is generally attributed to adhesion[12]. From Fig. 2, the calculated surface energy is close to that of water. This suggests that the hysteresis in the attractive regime is due to meniscus formation.

C. Effect of humidity and surface chemistry

C.1. Hydrophilic surface

Hydrophilic Si surfaces were exposed to increasing and then decreasing humidities between <2% and 80%. Although many humidity experiments were conducted, only the results for exposures from low to high to low humidities are presented here.

Figure 3a shows the interaction stiffness curve during approach and retraction for 2% RH (starting condition). As the sample approaches the tip, the tip is attracted to the surface due to long-range surface forces. The interaction stiffness is slightly negative before it becomes increasingly positive. Unlike the results in Fig. 2, there is no hysteresis in the attractive regime during retraction. The results are very reproducible and the same response is found up to a relative humidity of 50%. This suggests that there is no meniscus formation as expected for low humidity. Above 60% RH, hysteresis in the stiffness curves is seen during retraction, consistent with meniscus formation. Figure 3b shows the stiffness curve for 80% RH. After exposing the specimen to 80% RH, the humidity is reduced. Figure 3c shows the interaction stiffness curve when the relative humidity is reduced to 4%. Despite the low RH, residual meniscus formation was still evident, supposedly from residual liquid layers on the tip and surface.

From the interaction stiffness curve, the pull-off length during retraction can be measured. The pull-off length can be used as a characteristic measure of meniscus formation [12]. When there is no meniscus the pull-off length is zero. Figure 4 shows the pull-off length measured as a function of relative humidity during low-high-low humidity cycle for all the experiments. During the low-to-high portion of the cycle, the influence of humidity starts to appear around 60% RH and increases dramatically as the relative humidity approaches saturation. Our observations are similar to the results presented in the literature using AFM[12,13]. Once the surface is exposed to higher humidity, reducing the humidity decreases the pull-off length, but does not completely reduce to the value measured at the start of the experiment. This indicates that once the specimen is exposed to high humidity, water remains on the surface even after the humidity is reduced, illustrating the irreversible nature of water adsorption at room temperature on hydrophilic Si surfaces.

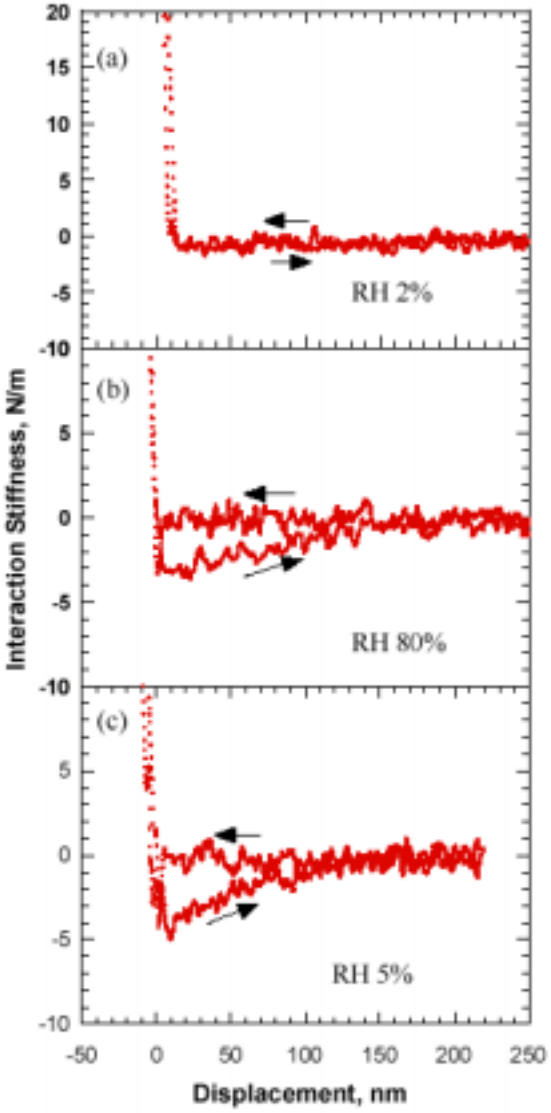

FIG.3. Influence of humidity on a hydrophilic Si surface: a) 2% RH, b) 80% RH and c) 5% RH.

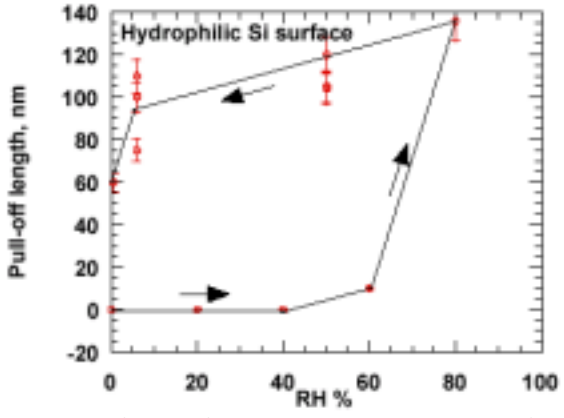

FIG.4. Influence of humidity on a hydrophilic Si surface showing irreversibility.

C.2. Hydrophobic surface

To investigate the effect of humidity on hydrophobic surfaces, interaction stiffness curves were measured on HF treated Si surfaces. Figure 5a shows the stiffness curve during approach and retraction for 5% RH. Both attractive and repulsive interactions were measurable even at relatively low humidity. Stiffness curves were similar up to a humidity level of 50%, above which interaction lengths began to increase. The length scale of maximum pull-off force measured for 95% RH is ~11 nm (Fig. 5b). Reducing the humidity back to 5% RH (high-to-low, Fig 5c) provided similar response observed in the start of the experiment. Figure 6 shows the variation of pull-off length as a function of humidity (summary of all the experimental data). The influence of humidity is very much reduced for the hydrophobic Si surface, and unlike hydrophilic surfaces (Fig. 4), the effect of exposure to humidity is reversible.

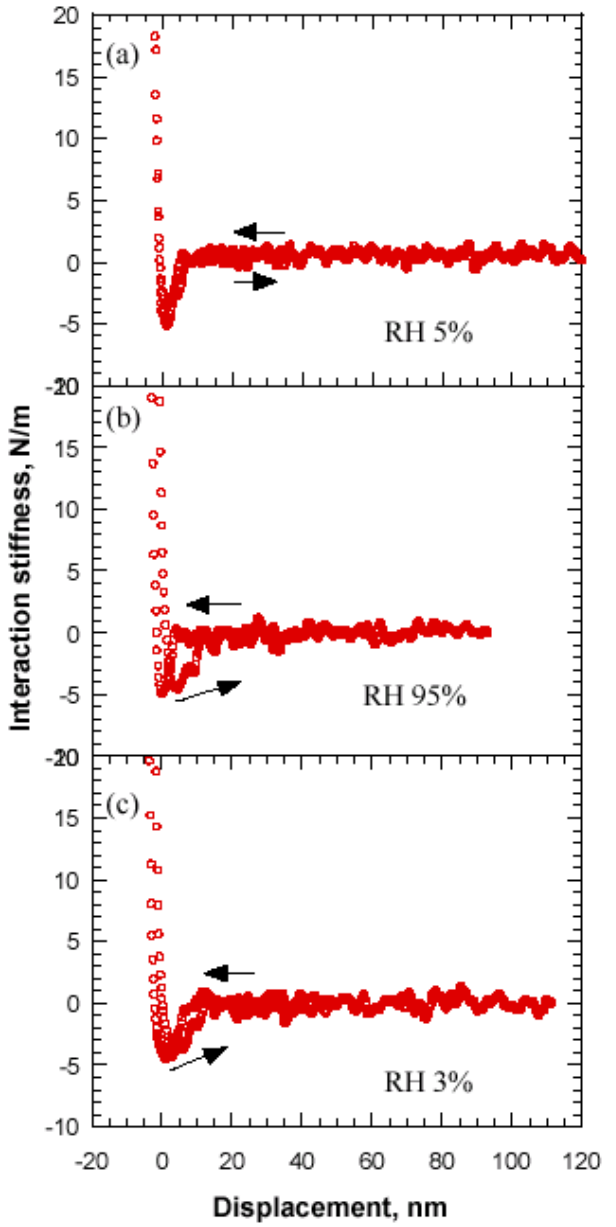

FIG. 5. The influence of humidity on a hydrophobic Si surface: a) 5% RH, b) 95% RH and 3% RH.

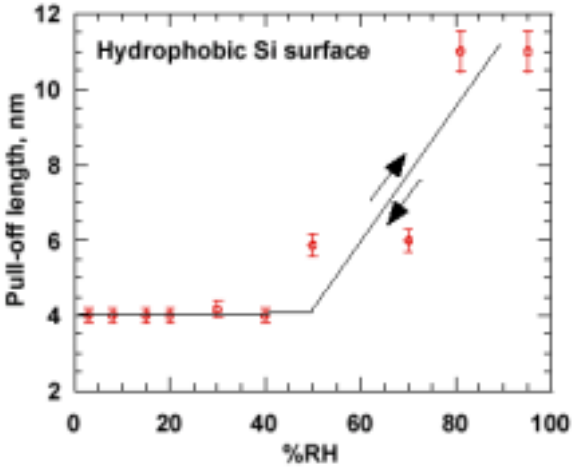

FIG. 6. Influence of humidity on a hydrophobic Si surface showing reversibility.

D. Elasto-plastic contact and nanoindentation

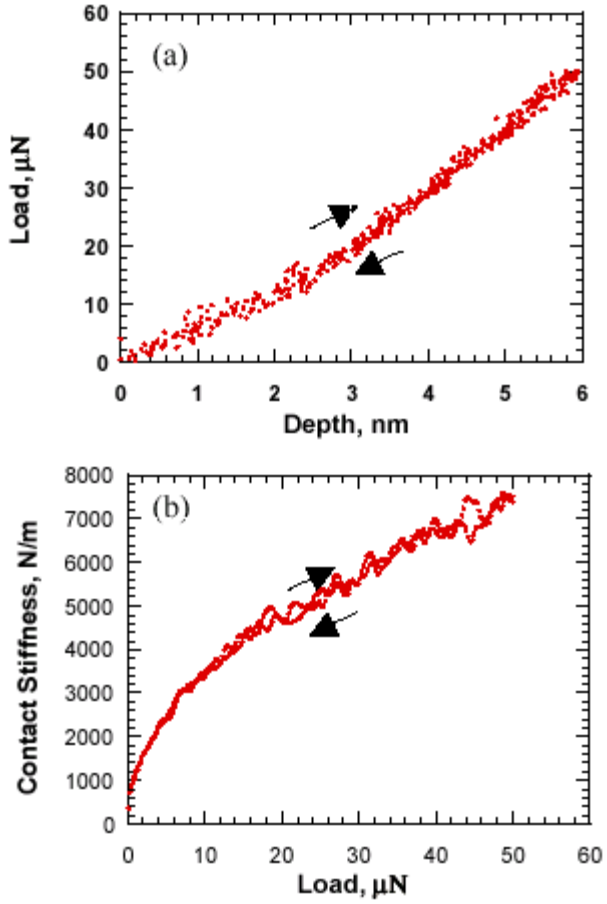

FIG. 7. The elastic loading and unloading of a hydrophilic Si surface: a) load-displacement curve and b) contact stiffness as a function of load.

Figure 7a shows the load-displacement curve for hydrophilic Si surface at 2-5 % RH. The sample is loaded to a maximum load of 50 μN and then unloaded. The corresponding contact stiffness curve is shown in Fig. 7b. The loading and unloading is reversible and the deformation is elastic. When the load is increased to 400 μN, there is a discontinuity generally known as "pop in", in the load-displacement response (Fig. 8a). This effect has been observed in other materials[14-16] as a critical load is reached. This has been attributed to a variety of mechanisms including sudden nucleation of dislocations, micro fracture, thin film debonding or oxide layer breakthrough. Pop-in can occur due to any process which results in sudden release of strain energy.

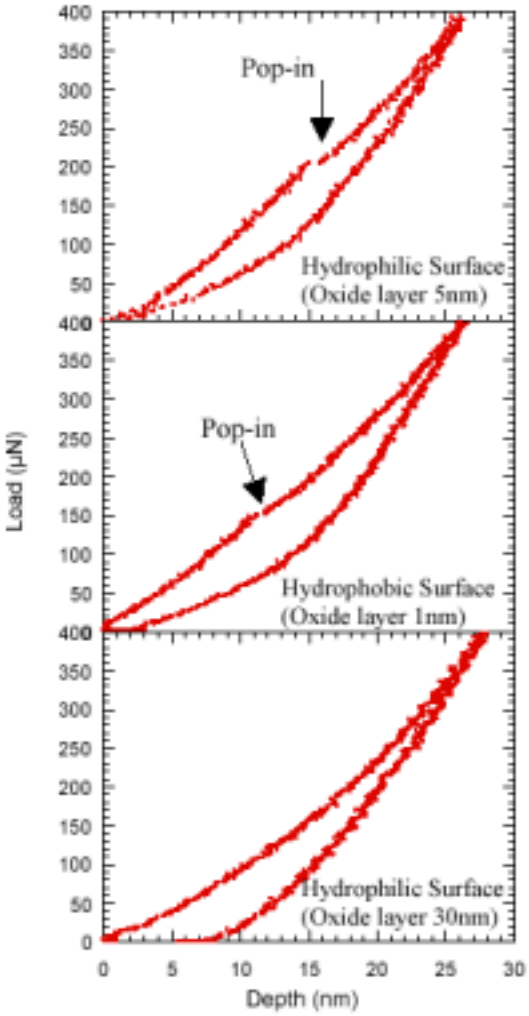

Fig. 8. The load-displacement response of Si surfaces showing pop-in and the influence of oxide layer thickness: a) hydrophilic Si surface with 5 nm oxide; b) hydrophobic Si surface with ~1 nm oxide; c) hydrophilic Si surface with 30 nm thermal oxide.

It should be noted that Si under hydrostatic pressure undergoes a pressure-induced phase transformation from a semiconductor (cubic diamond) to metallic (β-tin) state[17-18]. When the pressure is removed, the reverse transformation occurs at distinctly lower pressures. The hardness of Si is ~11 GPa[19], which is almost equal to the pressure required for phase transformation. Several investigators have shown that the inelastic deformation in silicon during indentation is dominated by a pressure-induced phase transformation[20-22]. During unloading of the indenter a distinct reverse thrust or pop-out is observed for higher load experiments (>50 mN),

which could be due to a reverse phase transformation. For relatively low-load experiments (<5 mN), pop-out is not found; instead a distinct hysteresis in the unloading curve is found. Most of the reported indentation work on Si is carried out at much higher loads (>1 mN) and the properties measured are that of the Si substrate rather than the oxide film. In the present work the experiments are carried out at much lower loads (~500 μN). In Fig. 8a the pop-in occurs reproducibly in the loading curve around 220 μN. Below this critical load, however the loading and unloading curve is reversible and the deformation is totally elastic (Fig. 7a and b).

Figure 8b shows the load-displacement curve for hydrophobic Si surfaces. The experiments were carried out at a relative humidity of 3 %. It can be seen that the pop-in event still occurs, but at a lower critical load ~150 μN. This could be due to the fact that HF etching does not completely remove the oxide layer. Hence, the thickness of the oxide layer apparently affects the pop-in behavior. To better understand the role of oxide thickness, several indentation experiments are carried out on 30 nm thick, thermally-grown SiO_2 on Si at various loads (10-1200 μN). Figure 8c shows the load-displacement response for indentation into this oxide layer. At a load of 400 μN the deformation is elasto-plastic and there is no evidence of pop-in. From the unloading curve the modulus and the hardness can be calculated[9] at different contact depths.

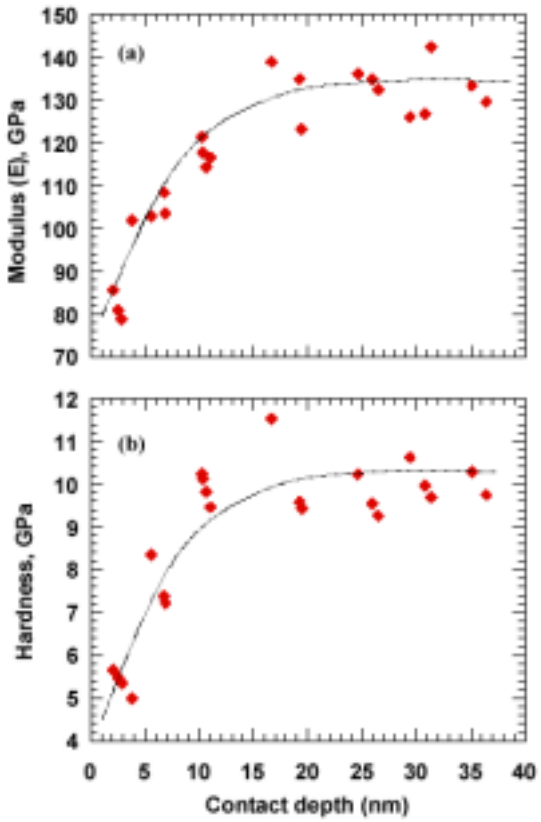

Fig. 9. Depth dependence of (a) modulus and (b) hardness of SiO_2 on Si substrate.

Figure 9a shows the variation of modulus as a function of contact depth, that is the depth at which the material conforms to the shape of the indenter. At higher contact depths (>15 nm), the measured modulus is 130-140 GPa. The measured modulus compares very well with the modulus of Si (134 GPa) reported in the literature[23]. At shallow contact depths (<15 nm), the modulus decreases and approaches 70-80 GPa for depths about 1-2 nm. The modulus of fused quartz (SiO_2) is ~70 GPa. This clearly indicates that at depths of ~1-2 nm the measured modulus is that of the oxide layer (SiO_2). Additionally, as the depth of indentation increases, substrate influence appears since the oxide layer is more compliant than the Si substrate.

Figure 9b shows the variation of hardness as a function of contact depth. The measured hardness has the same trend as the modulus. At shallow contact depth (1-2 nm) the hardness is ~5 GPa and it increases to 10-11 GPa at a contact depth of 12-15 nm and remains constant thereafter. As mentioned before, the hardness of Si is ~11 GPa which is almost equal to the pressure required for phase transformation. The hardness of the oxide layer is ~5 GPa (for a contact depth of 1-2 nm).

If the oxide layer is more compliant than the substrate, then why is the deformation prior to pop-in elastic but elasto-plastic after the pop-in? The influence of oxide layer on pop-in behavior and its thickness dependence can be explained by modeling the oxide layer on Si as a soft and compliant film on a hard and stiffer substrate (Fig. 10). The critical load required for pop-in depends on the tip radius of the indenter and thickness of the oxide layer. The tip radius of the indenter used in the present experiment is ~200 nm. When the load is applied on a very thin film (~1 nm for the HF etched surface), most of the load is supported elastically by the substrate until the mean contact pressure reaches ~11 GPa. The critical load required to reach this pressure is the pop-in load. When the mean pressure reaches 11 GPa, Si undergoes pressure-induced phase transformation and the load is no longer supported elastically by the substrate. The thin oxide film cannot accommodate the high strain induced by the plastic deformation of the Si substrate. This results in breakthrough of the oxide layer, which appears as a pop-in in the load-displacement data. If the thickness of the oxide layer is slightly larger (5 nm for the piranha-etched surface) then the substrate is further away from the surface, the load required to reach a mean contact pressure of 11 GPa increases and the pop-in occurs at higher load. However, for a thicker oxide layer (30 nm thermally-grown oxide) the substrate influence is significantly reduced and the plastic deformation occurs within the film itself. For a thicker oxide layer the pop-in may occur at relatively high loads but prior to pop-in the deformation is elasto-plastic. Thus the presence of a thicker oxide layer reduces the contact pressure and increases the load required for pressure-induced phase transformation of Si substrate.

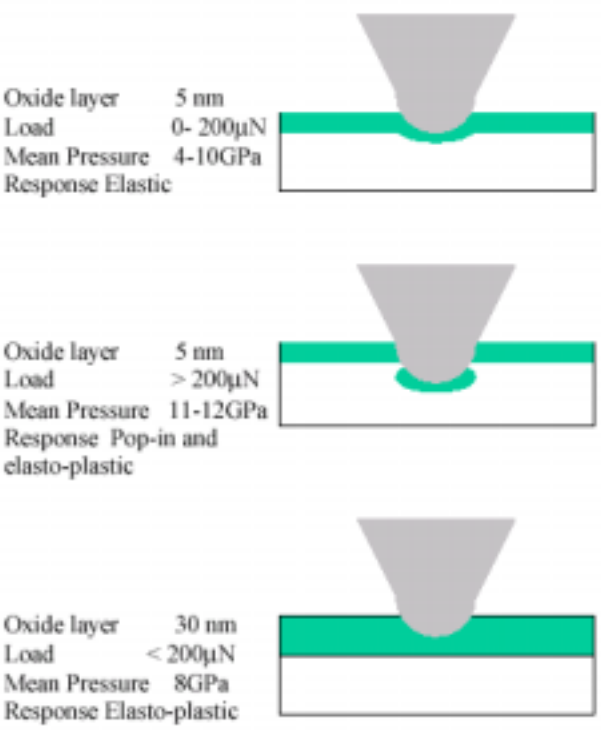

FIG. 10. Schematic model showing the influence of oxide layer thickness on pop-in behavior.

IV. CONCLUSIONS

By combining force modulation with depth sensing nanoindentation it is possible to measure the surface forces, surface energy, and interaction stiffness prior to contact. It is possible to locate the surface of the specimen without contact damage and the mechanical response of the surface layer can be measured. The hysteresis in the attractive regime during pull-off is due to meniscus formation. Once the hydrophilic Si surface is exposed to high humidity, meniscus formation remains even after the humidity is reduced. The influence of humidity is very much reduced for the hydrophobic Si surface and it is reversible.

In the contact regimes the irreversibility found at small loads (300 nN) is due to the deformation of the surface layer. For loads greater than 1 μN applied on thin oxide films, the deformation is elastic until the mean contact pressure reaches 11 GPa. At 11 GPa, Si undergoes pressure-induced phase transformation resulting in oxide layer breakthrough and pop-in. The critical load required for pop-in depends on the oxide layer thickness and the indenter tip radius. For thicker oxide layers the substrate influence is reduced and the plastic deformation occurs within the film itself without pop-in.

ACKNOWLEDGEMENTS

The authors thank Hysitron, Inc., Ken Lee, Jim Schneider and Steve Bullock for help and assistance with the experiments. S.A.S. Asif thanks the University of Florida for funding through a DOD/AFOSR MURI (#F49620-96-1-0026) Postdoctoral Fellowship. This work was supported in part by the Office of Naval Research.

REFERENCES

1. J.B. Pethica, R. Hutchings, and W.C. Oliver, Philos. Mag. A **48**, 593 (1983).
2. G.Binnig, C.F. Quate and Ch. Gerber, Phys. Rev. Lett. **56**, 930 (1986).
3. N.A. Burnham and R.J. Colton, J. Vac. Sci. Technol. A **7**, 2906 (1989).
4. N.A.Burnham, R.J. Colton and H.M. Pollock, Nanotechnology **4**, 64 (1993).
5. M.R. VanLandingham, S.H. McKnight, G.R. Palmese, J.R. Elings, X. Huang, T.A. Bogetti, R.F. Eduljee, and J.W. Gillespie, Jr., J. Adhesion **64**, 31 (1997).
6. S.A. Syed Asif, K.J. Wahl, and R.J. Colton, Rev. Sci. Instrum. **70**, 2408 (1999).
7. K.E. Petersen, Proc. IEEE **70**, 420 (1982).
8. M.R. Houston, R.T. Howe, and R. Maboudian, J. Appl. Phys. **81**, 3474 (1997).
9. W.C. Oliver and G.M. Pharr, J. Mater. Res. **7**, 1564 (1992).
10. O.P. Behrend, F. Oulevey, D. Gourdon, E. Dupas, A.J. Kulik, G. Gremaud, and N.A. Burnham, Appl. Phys. A. **66**, S219 (1998).
11. J.N. Israelachvili and D. Tabor, Proc. R. Soc. London, Ser. A **331**, 19 (1972).
12. M. Binggeli and C.M. Mate, Appl. Phys. Lett. **65**, 415 (1994).
13. J. Hu, X.-D. Xiao, D.F. Ogletree, M. Salmeron, Science **268**, 267 (1995).
14. S.A. Syed Asif and J.B. Pethica, Philos. Mag. A **76**, 1105 (1997).
15. S.G. Corcoran, R.J. Colton, E.T. Lilleodden and W.W. Gerberich, Phys. Rev. B **55**, R16057 (1997).
16. A.B. Mann and J.B. Pethica, Philos. Mag. A **79**, 577 (1999).
17. H. Minomura and H.G. Drickamer, J. Phys. Chem. Solids **23**, 451 (1962).
18. M.C. Gupta and A.L. Ruoff, J. Appl. Phys. **51**, 1072 (1980).
19. J.Z. Hu, L.D. Merkle, C.S. Menoni, and I.L. Spain, Phys. Rev. B **34**, 4679 (1986).
20. A.P. Gerk and D. Tabor, Nature **271**, 732 (1978).
21. D.R. Clarke., M.C. Kroll, P.D. Kirchner, R.F. Cook, and B.J. Hockey, Phys. Rev. Lett. **60**, 2156 (1988).
22. G.M. Pharr, W.C. Oliver and D.S. Harding, J. Mater. Res. **6**, 1129 (1991).
23. C.J. Smithells, *Smithells Metal Reference Book*, edited by E.A. Brandes (Butterworths, London, 1983), 6th ed., p. 15.